PHOSPHATE NODULES CONTAINING TWO DISTINCT ASSEMBLAGES IN THE CEMA GRANITIC PEGMATITE, SAN LUIS PROVINCE, ARGENTINA: PARAGENESIS, COMPOSITION AND SIGNIFICANCE

Encarnación RODA-ROBLES[§]

Departamento de Mineralogía y Petrología, Univ. País Vasco (UPV/EHU), P.O. Box 644, E–48080 Bilbao, Spain

Miguel A. GALLISKI

IANIGLA, CCT–MENDOZA CONICET, Avda. Ruiz Leal s/n, Parque Gral. San Martín, C.C. 330, (5.500) Mendoza, Argentina

M. Belén ROQUET

Departamento de Geología, Universidad Nacional de San Luis, Chacabuco y Pedernera, San Luis, Argentina

Frédéric HATERT

Laboratoire de Minéralogie, B18, Université de Liège, B–4000 Liège, Belgium

Philippe de PARSEVAL

Université de Toulouse, UPS (OMP), CNRS, IRD–GET, 14, avenue Edouard Belin, F–31400 Toulouse, France

Abstract

Nodules of Fe–Mn phosphates are common in the outer core zone of the Cema pegmatite, San Luis Range, Argentina. Two different complex phosphates associations have been distinguished in these nodules. One of them is beusite–wyllieite–sicklerite-rich (BWS), with varulite and staněkite among the main products of replacement, Fe/(Fe + Mn) values between 0.46 and 0.48 for sicklerite, and MgO values up to 2.14 wt%. The other association is lithiophilite–sicklerite-rich (LS), with varulite and hureaulite among the main secondary products, lower Fe/(Fe + Mn) values, in the range 0.37–0.39 for lithiophilite, and lower MgO contents, invariably below 1 wt%. According to the mineral-chemistry data of these Fe–Mn phosphate nodules, a higher temperature of crystallization is proposed for the BWS association compared to the LS one. The Mn enrichment observed in these phosphates, in a pegmatite that is not highly fractionated, could be explained as a result of the early crystallization of other Fe–(Mg–Mn)-rich minerals, such as schorl, in the border and wall zones of this pegmatite. The crystallization of this silicate would have strongly depleted the activity of Fe in the remaining pegmatite-forming melt.

Keywords: Fe–Mn phosphates, nodules, mineral compositions, granitic pegmatites, Cema, San Luis Range, Argentina.

Introduction

Phosphates of Fe–Mn and Al are common mineral phases in many granitic pegmatites. They are the main constituents in the beryl – columbite – phosphate subtype of the beryl type, REL–Li subclass of Černý & Ercit (2005). The presence of phosphates in evolved granites and pegmatites is not only due to the solubility of P in granitic melts and hydrothermal fluids, but also to the behavior of P as an incompatible element due to

the low activity of Ca in perphosphorous melts (those with more P_2O_5 than CaO to form normative apatite: Bea *et al.* 1992). The chemical composition of phosphates has frequently been used to establish the degree of evolution of the pegmatites in which they occur, with the Fe/(Fe + Mn) values decreasing as the degree of fractionation of the pegmatite increases (Ginsburg 1960, Fransolet *et al.* 1986, Keller 1994, Keller *et al.* 1994, Roda *et al.* 2005, Roda-Robles *et al.* 2010). Phosphates have usually been investigated independently

§ *E-mail address*: encar.roda@ehu.es

from the other coexisting minerals, such as silicates or oxides; as a consequence, it is not easy to interpret their chemical composition, and even the textures of some phosphates associations, as they may be conditioned by the presence of other Fe–(Mg–Mn)-rich minerals, such as tourmaline, biotite and garnet.

In the northeastern part of the San Luis Range, in Argentina, bodies of granitic pegmatite are common. Many of them are enriched in phosphorus, and commonly show phosphate nodules in which complex associations occur (Hurlbut & Aristarain 1968, Oyarzábal & Galliski 2007, Galliski *et al.* 2009, Roda-Robles *et al.* 2009). In this study, the phosphate associations of the Li–Be–P–B-bearing Cema pegmatite are described; we take into account their textural features and chemical compositions. Moreover, we give an interpretation of the role played by the phosphate phases in the internal evolution of the pegmatite and discuss the possible influence of other Fe–(Mg–Mn)-bearing minerals on the chemical composition of the phosphates that we investigated.

GEOLOGICAL SETTING AND GENERAL GEOLOGY OF THE PEGMATITE

The Li–Be–P–B-bearing Cema granitic pegmatite is located at 32°34'52" S and 65°24'51" W, in the Department of Libertador General San Martín. This pegmatite belongs to the Conlara pegmatite field, situated in the northern part of the Eastern Pampean Ranges of San Luis (Galliski 1994). The crystalline basement in this part of the range is composed of Eopaleozoic rocks belonging to the Conlara Metamorphic Complex (Sims *et al.* 1997), and dominantly of gneisses, metapelites and mica schists. During the Ordovician, these rocks were intruded by S-type granites and the associated pegmatitic bodies. The Cema pegmatite mainly intrudes into gray mica schists, and also partly into a dioritic lens in its northwestern part.

The Cema pegmatite is a discordant body, with a N–S strike, dipping 52° to the southwest. It has an irregular shape, with a length of 100 m and a thickness difficult to estimate, as only the upper part of the pegmatite crops out (Roquet 2010). Taking into account the thicknesses of the different structural units, the whole pegmatite seems to be rather thin, only a few meters between the contacts. The Cema body presents a complex inner zonation, with an asymmetric development. The following zones have been recognized (Table 1, Fig. 1): border zone, wall zone, intermediate zone and core zone, in addition to a core–rim assemblage and two replacement units. The presence of Fe–(Mg–Mn)-rich silicates like tourmaline (schorl) and garnet (spessartine) in the border and in the wall zones is remarkable. It is also noteworthy that spodumene crystals, up to 40 cm in length, are common in the quartz-dominant core zone. The phosphates occurring in the Cema pegmatite are associated with the outer core zone, where they

appear together with subhedral crystals of beryl. Finally, two distinct replacement units have been distinguished in the Cema pegmatite (Roquet 2010). The first one is albite-rich, and could be related to an episode of Na metasomatism after the primary crystallization of the pegmatite, at a subsolidus stage. The second one, muscovite-rich, could have developed during a hydrothermal stage of greisen formation, presumably at an even lower temperature. The pegmatite has a mineralogy compatible with the spodumene subtype of complex type, REL–Li subclass, in the classification scheme of Černý & Ercit (2005). Approximately 200 m to the south–southwest of the Cema pegmatite, a lenticular body of pegmatitic leucogranite crops out, which is mined for ceramic materials at present. This is a mica-rich coarse-grained granite in which a graphic texture is prominent. More recent exploitations located 250 m to the west–northwest show an extensively albitized tourmaliniferous leucogranite. One of these granitic bodies could be the parental granite of the Cema pegmatite, but at the present level of knowledge, this hypothesis cannot be tested. Nevertheless, these intrusive bodies are petrographically similar to the small stocks or lenses of leucogranites that belong to an S-type suite of mostly Ordovician late-orogenic granites, which are interpreted as the parental bodies of the LCT pegmatites of the Pampean pegmatite province (Galliski 2009).

TABLE 1. MAIN CHARACTERISTICS OF THE UNITS
IN THE CEMA GRANITIC PEGMATITE

| Zone	Thickness	Mineralogy	Grains size	Comments
Border	5-15 cm	Qtz 50% Ab 30% Ms 10% Tur 8% Grt+Ap 2%	Very fine to fine	Discontinuous mainly in the E and W walls Whitish Ms, Tur ⊥ contacts
Wall	20-60 cm	Ab 40% Qtz 30% Ms 20% Tur+Grt +Ap 10%	Medium	Whitish Coarser grain-size Ms ⊥ interm. zone
Intermediate	variable	Qtz 60% Ksp 40%	Coarse	Pinkish Blocky Qtz, Ksp
Outer core	variable	Beryl Phosphate nodules	Medium to coarse	Brl crystals ≈10cm Phosphate nodules 0.1-1 m in diameter
Core center	< 3m	Qtz 80% Spd 20%	Coarse	Whitish Largest outcrop in the open pit
Replacement units	variable	Ab 60% Ms 20% Qtz 10% Gr 5% Tur 5% Grt+Ap 2%	Very fine to medium	Developed over various zones of the pegmatite
	1-3 m × 1-7 m	Ms + Qtz	Very fine to fine	Greisen bodies of irregular shape
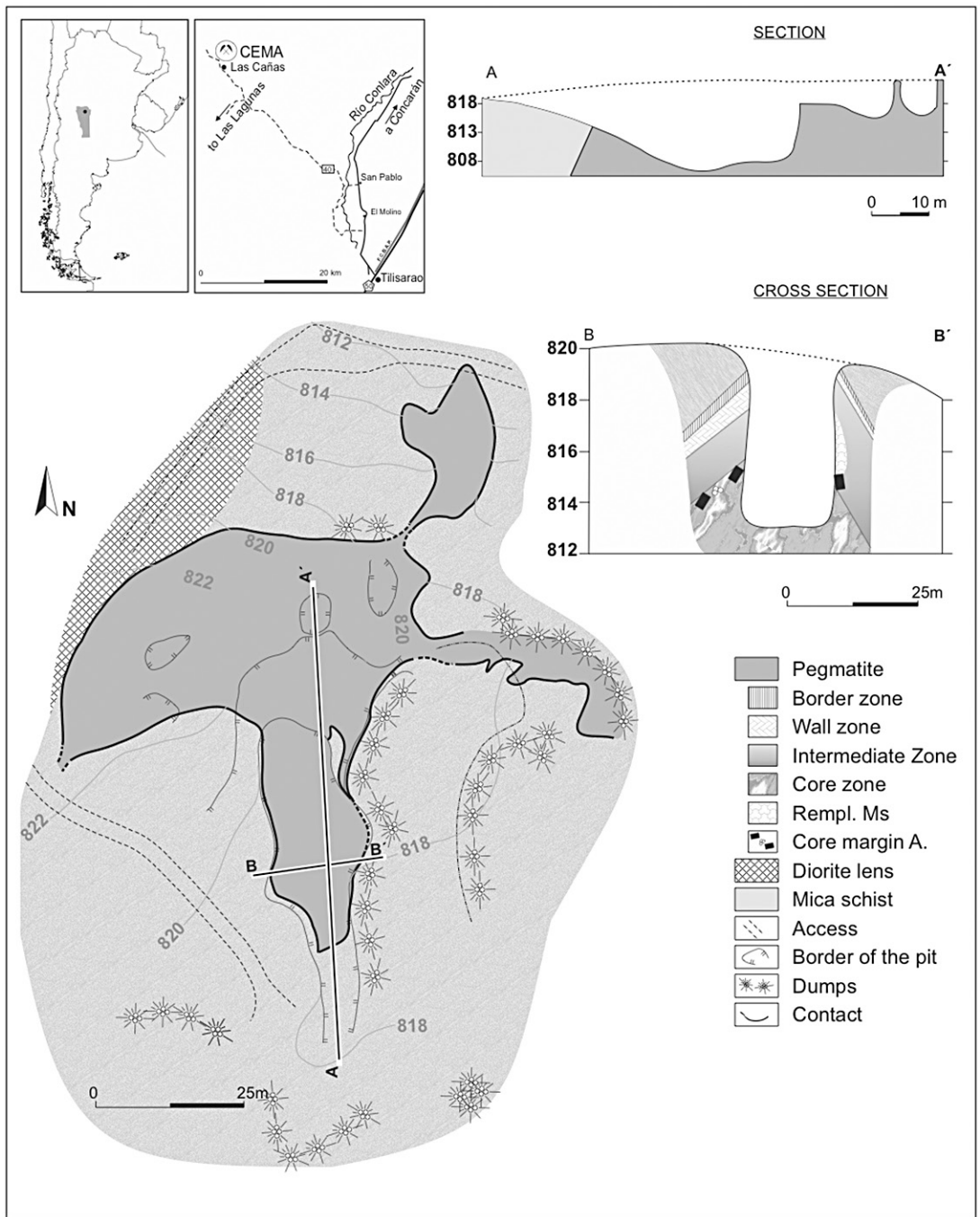
Fig. 1. Schematic geological map of the Cema pegmatite, San Luis Province, Argentina, and idealized cross-sections, as indicated in the map.

DATA COLLECTION AND ANALYSES

Several phosphate samples were collected *in situ* from different nodules belonging to the outer core zone. In addition, some tourmaline and garnet crystals from the wall and border zones have been studied. Mineral identification of the phosphates, tourmaline and garnet has been carried out by a study of their optical properties in thin section, X-ray powder-diffraction techniques, and electron-microprobe analyses. More than 250 chemical analyses on phosphates were performed at the Université Paul Sabatier (Toulouse, France), with a Cameca SX50 electron microprobe. The operating conditions were: voltage 15 kV, beam current 10 nA for phosphates and tourmaline, and 20 nA for garnet for all elements. The internal standards used for the phosphates are natural minerals except for Pb (see below): $PK\alpha$ (graftonite), $AlK\alpha$ (corundum), $FeK\alpha$ (hematite), $MnK\alpha$ (pyrophanite), $MgK\alpha$ (periclase), $CaK\alpha$ and $SiK\alpha$ (wollastonite), $KK\alpha$ (sanidine), $NaK\alpha$ (albite), $SK\alpha$ (celestine), $BaL\alpha$ (barite), and $PbM\beta$ (synthetic $Pb_2P_2O_7$).

For the tourmaline, we used natural minerals as standards: $CaK\alpha$ and $SiK\alpha$ (wollastonite), $TiK\alpha$ and $MnK\alpha$ (pyrophanite), $AlK\alpha$ (corundum), $CrK\alpha$ (Cr_2O_3), $FeK\alpha$ (hematite), $MgK\alpha$ (periclase), $ZnK\alpha$ (sphalerite), $NaK\alpha$ (albite), $KK\alpha$ (sanidine) and $FK\alpha$ (topaz). For garnet, we used natural minerals: $CaK\alpha$ and $SiK\alpha$ (wollastonite), $TiK\alpha$ and $MnK\alpha$ (pyrophanite), $AlK\alpha$ (corundum), $CrK\alpha$ (Cr_2O_3), $FeK\alpha$ (hematite), $MgK\alpha$ (periclase), $ZnK\alpha$ (sphalerite), $NaK\alpha$ (albite) and $KK\alpha$ (sanidine).

PETROGRAPHY AND COMPOSITION
OF THE PHOSPHATES

In the Cema pegmatite, phosphates are restricted to the outer core zone, where subhedral beryl crystals, up to 10 cm in size also are common. The phosphates occur as yellowish to dark rounded, ellipsoidal and, more rarely, angular masses, 0.1 to 1 m across, mainly inside the quartz and, less commonly, inside the blocky K-feldspar (Fig. 2). More than twenty phosphate minerals have been identified in the Cema pegmatite. Ideal formulae and abundances are given in Table 2. It is remarkable that in general, these phosphates are mostly Mn-rich, with lower contents in Fe, and relatively high Mg contents for some of them. Many of the identified phosphates correspond to late or secondary phosphates; however, some primary and early secondary phosphates also occur, such as lithiophilite, beusite, triploidite, sicklerite, wyllieite, dickinsonite-(KMnNa), staněkite, and varulite.

Two different phosphate associations may be distinguished in the Cema suite. In the so-called BWS association, lithiophilite has not been found, and the main phosphates are beusite, wyllieite and sicklerite, whereas in the LS association, lithiophilite and sicklerite are abundant. Nodules containing the two different phosphate associations appear scattered in the core margin of the pegmatite, without a pattern of distribution being evident.

FIG. 2.   View of some phosphate nodules in the outer core zone of the Cema pegmatite, San Luis Province, Argentina.
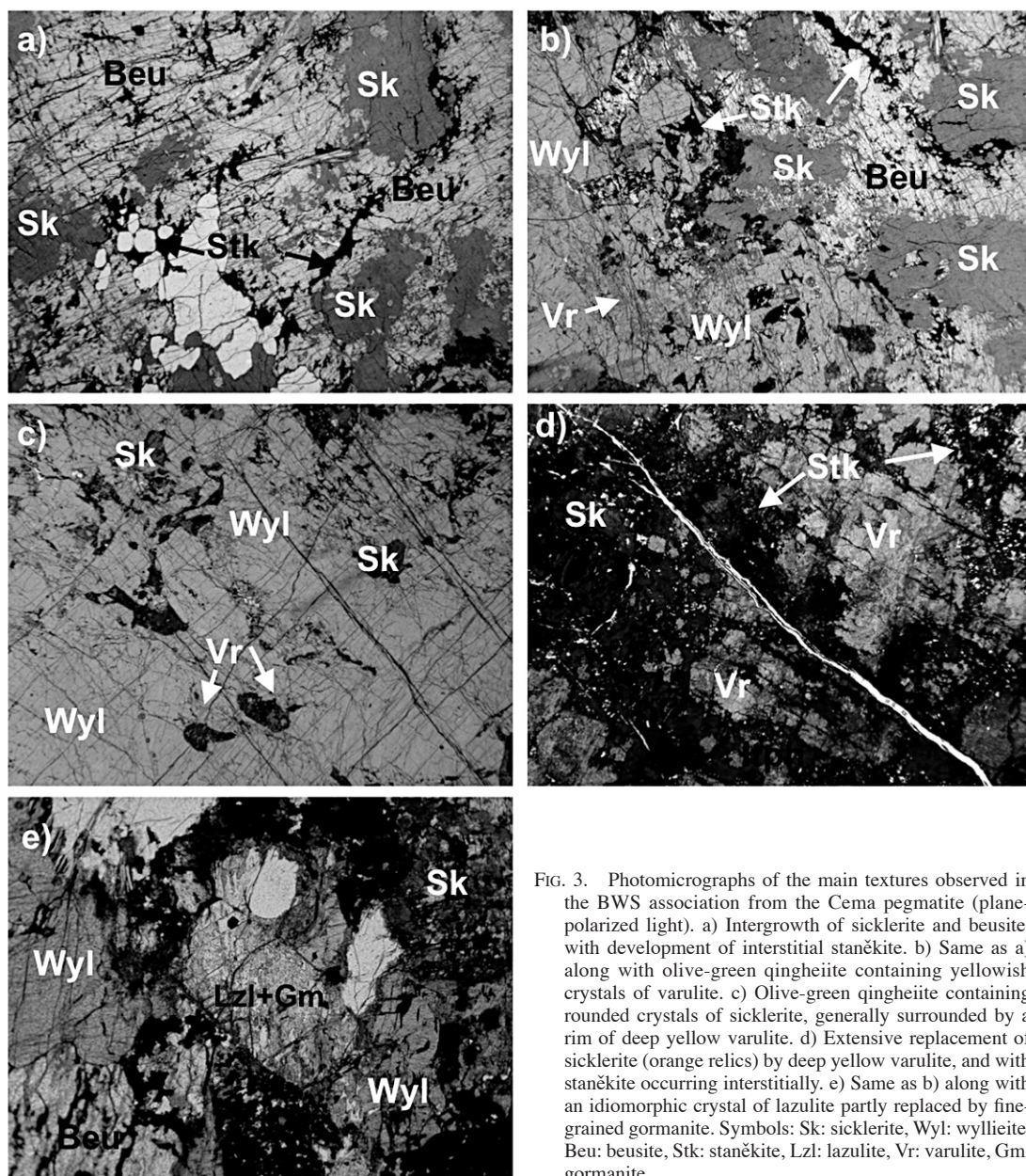
FIG. 3. Photomicrographs of the main textures observed in the BWS association from the Cema pegmatite (plane-polarized light). a) Intergrowth of sicklerite and beusite, with development of interstitial staněkite. b) Same as a) along with olive-green qingheiite containing yellowish crystals of varulite. c) Olive-green qingheiite containing rounded crystals of sicklerite, generally surrounded by a rim of deep yellow varulite. d) Extensive replacement of sicklerite (orange relics) by deep yellow varulite, and with staněkite occurring interstitially. e) Same as b) along with an idiomorphic crystal of lazulite partly replaced by fine-grained gormanite. Symbols: Sk: sicklerite, Wyl: wyllieite, Beu: beusite, Stk: staněkite, Lzl: lazulite, Vr: varulite, Gm: gormanite.

The beusite–wyllieite–sicklerite (BWS) association

In this association, lithiophilite has not been detected up to now, and sicklerite is the most abundant phase. It mainly occurs as anhedral crystals giving a granular texture, generally intergrown with colorless, anhedral beusite (Figs. 3a, b). Another common phase in the BWS association is wyllieite. It appears as deep olive green masses of anhedral crystals, close to the sicklerite–beusite intergrowths (Fig. 3b) or hosting very fine-grained, subrounded grains of sicklerite. In that case, it is quite common that this sicklerite is partially replaced by deep yellow varulite that occurs as a rim between the wyllieite and the sicklerite (Fig. 3c). In other cases, varulite replaces extensively the granular sicklerite (Fig. 3d), and forms small subhedral crystals

inside wyllieite. The occurrence of some very fine grains of lazulite close to wyllieite is noteworthy; these show a deep bluish color and are partially replaced by gormanite (Fig. 3e). Dickinsonite-(KMnNa) is another early phase identified in the BWS association, forming very fine-grained subhedral to euhedral crystals enclosed in wyllieite or sicklerite. Another early product of replacement in the BWS association is staněkite, which commonly occurs as very fine-grained crystals showing a very dark brownish color, and located interstitially between the sicklerite crystals (Figs. 3a, b and d).

Later secondary phases occurring in the BWS include eosphorite, pararobertsite and gormanite (Table 2). Their main petrographic characteristics are summarized in Table 3.

Overall, the primary and early secondary phosphates from the BWS association are richer in Mn than in Fe, with relatively high Mg contents for some of them (Tables 4, 5 and 6, Fig. 4a). Consequently, sicklerite shows Fe/(Fe + Mn) values in the range 0.38–0.49, and MgO contents up to 2.14 wt.% (mean 1.94 wt.%) (Table 4). Varulite inherits the Fe–Mn–Mg proportions of the parent phase, presumably sicklerite, with Fe/(Fe + Mn) in the range 0.35–0.49, and MgO values up to 5.43 wt.% (mean 1.73 wt.%) (Table 5). Wyllieite, with Fe/(Fe + Mn) in the range 0.36–0.40, shows the highest

MgO values (up to 4.6 wt.% and a mean value of 3.7 wt.%) (Table 6). Beusite is the phase richest in Mn and poorest in Mg of all the early phosphates in the BWS association, as has been described in other phosphates associations (Roda-Robles *et al.* 2011) (Table 3). Its Fe/(Fe + Mn) value is in the range 0.34–0.35, with MgO values invariably below 0.65 wt.%.

Staněkite is the early phosphate richest in Fe in the BWS association, with Fe/(Fe + Mn) values ranging between 0.53 to 0.59 (Table 3, Fig. 4a). Finally, dickinsonite-(KMnNa) shows intermediate values of Fe/(Fe + Mn), ranging from 0.41 to 0.42 (Table 4).

The lithiophilite–sicklerite (LS) association

In this association, colorless lithiophilite is abundant, generally replaced partially by orange to yellowish sicklerite. In some crystals, the contact between these two phases is sharp, with a sudden change in color (under plane-polarized light). However, in some other crystals, the color change is gradual, from colorless lithiophilite, through light and deep yellow, to deep orange sicklerite (Fig. 5a). In general, both minerals appear as anhedral fine-grained crystals but, in some cases, elongate areas are observed inside these minerals themselves, where they appear with a very fine-grained granular texture, where grain boundaries intersect at ~120° triple junctions (Figs. 5b, c).

Lithiophilite and sicklerite are also replaced by varulite. Where this replacement is incipient, it follows the cleavage planes of these olivine-type phosphates, as previously observed during the replacement of triphylite and ferrisicklerite by alluaudite-type phosphates (Huvelin *et al.* 1972, Boury 1981, Fransolet *et al.* 1985). Where replacement is more extensive, varulite appears as patches inside the lithiophilite or the sicklerite, as aggregates of fibroradial crystals.

Another primary phosphate phase in the LS association is triploidite, which forms anhedral colorless grains associated with lithiophilite and reddingite. Wyllieite is very scarce in this association, and appears as anhedral to subhedral, very fine-grained crystals of deep-olive color, interstitial between some lithiophilite crystals (Fig. 5d).

Other secondary phases occurring in the LS association, replacing the lithiophilite and presumably crystallized at lower temperatures, include hureaulite, lipscombite, jahnsite-(CaMnMg), leucophosphite, rockbridgeite and dufrénite, among others (Table 2). Their main petrographic characteristics are summarized in Table 3.

In the LS association, all the primary and early secondary phosphates are richer in Mn than phosphates from the BWS association, as shown by lower Fe/(Fe + Mn) values and lower Mg contents (Tables 4, 5, 6, Fig. 4b). As a consequence, the primary phases lithiophilite and triploidite present Fe/(Fe + Mn) values in the ranges

TABLE 2. LIST OF THE PHOSPHATE MINERALS
IDENTIFIED IN THE CEMA PEGMATITE

Mineral	Formula	Association LS	BWS
Lithiophilite	$Li(Mn,Fe)PO_4$	++++	o
Sicklerite	$Li_{1-x}(Mn_{1-x}Fe^{3+}_x)PO_4$	++++	++++
Beusite	$(Mn,Fe^{2+}Ca)_3(PO_4)_2$	o	+++
Triploidite	$(Mn,Fe)_2(PO_4)OH$	+	o
Wyllieite	$Na_2MnFe^{2+}Al(PO_4)_3$	+	++
Dickinsonite-(KMnNa)	$KNa_4Ca(Mn,Fe^{2+})_{14}$ $Al(PO_4)_{12}(OH)_2$	o	+
Lazulite	$MgAl_2(PO_4)_2(OH)_2$	o	+
Varulite	$NaCaMn(Mn,Fe^{2+})_2(PO_4)_3$	+++	+++
Staněkite	$Fe^{3+}(Mn^{2+},Fe^{2+})(PO_4)O$	o	++
Apatite	$Ca_5(PO_4)_3(F,OH,Cl)$	o	+
Hureaulite	$Mn_5(PO_4)_2[PO_3(OH)]_2\cdot4H_2O$	+++	o
Eosphorite	$(Mn,Fe)Al(PO_4)(OH)_2\cdot H_2O$	o	+
Rockbridgeite	$(Fe,Mn)^{2+}Fe^{3+}_4(PO_4)_3(OH)_5$	++	o
Jahnsite	$CaMn(Mg,Fe^{2+})_2Fe^{3+}_2$ $(PO_4)_4(OH)_4\cdot8H_2O$	++	o
Lipscombite	$(Fe^{2+},Mn)Fe^{3+}_2(PO_4)_2(OH)_2$	+	o
Gormanite	$(Fe^{2+},Mg)_3(Al,Fe^{3+})_4$ $(PO_4)_4(OH)_6\cdot2H_2O$	o	+
Leucophosphite	$KFe_2(PO_4)_2(OH)\cdot2H_2O$	+	o
Phosphoferrite	$(Fe^{2+},Mn)_3(PO_4)_2\cdot3H_2O$	+	o
Reddingite	$(Mn,Fe)_3(PO_4)_2\cdot3H_2O$	+	o
Robertsite	$Ca_2Mn^{3+}_3(PO_4)_3O_2\cdot3H_2O$	o	+
Tavorite	$LiFe^{3+}(PO_4)(OH)$	+	o
Dufrénite	$Ca_{0.5}Fe^{2+}(Fe^{3+})_5$ $(PO_4)_4(OH)_6\cdot2H_2O$	+	o

LS: lithiophilite–sicklerite association; BWS: beusite–wyllieite–sicklerite association. The abundance in each association is given as: ++++: abundant, +++: commonly present, ++: rare, +: very rare, o: absent or not found.

0.36–0.39 and 0.22–0.34, respectively (Table 4). Lithio-philite and its replacement products, sicklerite and varu-lite, show similar Fe/(Fe + Mn) values (0.36–0.39), and MgO values invariably lower than 1 wt.% (Tables 4, 5). Wyllieite shows lower Fe/(Fe + Mn) values (0.34–0.35), and constitutes the phase richest in Mg in the LS asso-ciation, with a mean MgO value of 1.84 wt.%, locally reaching 2.70 wt.% (Table 6).

Most of the later secondary phases are, on the contrary, richer in Fe than in Mn, with Fe/(Fe + Mn) values in the range 0.68–0.80 for rockbridgeite, 0.79–0.82 for phosphoferrite, 0.89–0.92 for lipscombite, 0.59–0.61 for tavorite, and 0.61 for jahnsite-(CaMnMg) (Table 7).

PETROGRAPHY AND COMPOSITION OF TOURMALINE AND GARNET

Tourmaline and garnet are mainly present in the outer zones of the Cema pegmatite. They commonly occur in close association with muscovite, K-feldspar and albite. Muscovite appears as coarse book-type crystals (5–7 cm long). Muscovite sheets are inter-grown with a matrix of K-feldspar ± albite and quartz. Brownish to reddish garnet crystals are included in this matrix. Garnet crystals are quite broken, giving rise to anhedral masses of up to 5–6 cm. They also may appear as subhedral crystals, up to 1 cm across. The masses of garnet contain black prismatic crystals of schorl,

TABLE 3. MAIN PETROGRAPHIC CHARACTERISTICS OF THE MINERALS
OF THE BWS AND LS ASSOCIATIONS

Mineral	Habit, textures and color	Grain size	Fe/(Fe + Mn)	Associated minerals
Primary phosphates, BWS association				
Beusite	Granular Anhedral habit Colorless	Very fine to fine	0.34-0.35	Sk, Wyl, Vr, Stk, Lzl
Wyllieite	Granular Anhedral habit Colorless	Very fine to fine	0.36-0.40	Sk, Beu, Vr, Stk, Lzl, Dcn
Dickinsonite-(KMnNa)	Sub- to euhedral Inside Wyl and Sk Colorless to light green	Very fine to fine	0.41-0.42	Wyl, Vr, Sk
Lazulite	Euhedral Deep blue	Very fine	0.91-0.99	Beu, Wyl, Sk, Gm
Early secondary phases, BWS association				
Sicklerite	Granular Orange, yellowish	Very fine to fine	0.38-0.49	Beu, Vr, Wyl, Stk, Lzl, Eos, Ap, Dcn
Varulite	Cellular, fibroradial Deep yellow to reddish	Very fine	0.35-0.49	Sk, Vr, Wyl, Stk, Eos, Ap
Stan kite	Anhedral, interstitial Dark brown-black	Very fine	0.53-0.58	Beu, Sk, Wyl, Vr
Apatite	Anhedral Colorless to deep blue	Very fine		Sk, Vr, Ap
Late secondary phases, BWS association				
Eosphorite	Anhedral, fibroradial Beige-orange-yellow	Very fine	0.13-0.33	Vr, Sk, Ap, Stk
Gormanite	Anhedral Replacing lazulite Blue to colorless	Very fine	0.79-0.81	Lzl, Beu, Wyl, Sk
Robertsite	Anhedral Orange to reddish	Very fine	0.37-0.68	Vr, Sk

TABLE 3 (cont'd). MAIN PETROGRAPHIC CHARACTERISTICS OF THE MINERALS
OF THE BWS AND LS ASSOCIATIONS

Mineral	Habit, textures and color	Grain size	Fe/ (Fe + Mn)	Associated minerals
Primary phosphates, LS association				
Lithiophilite	Granular Anhedral habit Colorless	Very fine to medium	0.36-0.39	Sk, Vr, Hur, Rck, Lcb, Jhn, Tp, Wyl, Ms, Pl
Triploidite	Anhedral habit Colorless	Very fine to medium	0.22-0.34	Rdd, Lph
Wyllieite	Interstitial Subhedral habit Deep olive green	Very fine	0.34-0.35	Lph, Sk, Lcb
Early secondary phases, LS association				
Sicklerite	Granular Anhedral habit Orange, yellowish	Very fine to medium	0.36-0.39	Lph, Vr, Hur, Rck, Lcb, Jhn, Tp, Wyl, Ms, Pl
Varulite	Cellular, fibroradial Anhedral habit Deep yellow	Very fine to fine	0.34-0.42	Lph, Sk, Hur, lcph, Ms, Pl
Hureaulite	Sub- to euhedral Prismatic, Strong pleochroism Colorless to pinkish	Very fine to fine	0.00-0.18	Lph, Sk, Rck, Lcb, Vr, Jhn, Rdd
Lipscombite	Anhedral habit Dark greenish black	Very fine to fine	0.89-0.92	Lph, Sk, Vr, Hur, Rck, Hur, Jhn, Rck, Rdd
Late secondary phases, LS association				
Rockbridgeite	Subhedral habit Fibrous radial Brown-green	Very fine to fine	0.68-0.80	Lph, Sk, Hur, Lcb, Jhn
Jahnsite-(CaMnMg)	Euhedral habit Prismatic Yellowish color Filling cavities	Very fine to fine	0.84-0.89?	Lph, Hur, Drf, Rck
Leucophosphite	Rounded shapes Purple-violet	Very fine	0.35-0.81	Sk, Vr
Phosphoferrite	Anhedral habit Dark brown	Very fine	0.80-0.82	Lph, Vr, Lcb
Reddingite	Euhedral Pinkish, orange	Very fine to medium	0.28-0.29	Lph, Tp, Hur, Lcb
Tavorite	Anhedral habit Yellowish color	Very fine	0.59-0.61	Sk, Lph, Vr, Rck, Hur, Lcb
Dufrénite	Sub- to euhedral Fibroradial Strong pleochroism Dark green-brownish	Very fine	-	Lph, Hur, Jhn

Symbols used: Ap: apatite, Beu: beusite, Dcn: dickinsonite, Drf: dufrénite, Eos: eosphorite, Gm: gormanite, Hur: hureaulite, Jhn: jahnsite, Lzl: lazulite, Lcb: lipscombite, Lph: lithiophilite, Ms: muscovite, Pl: plagioclase, Rdd: reddingite, Rck: rockbridgeite, Sk: sicklerite, Stk: staněkite, Tp: triploidite, Vr: varulite, Wyl: wyllieite.
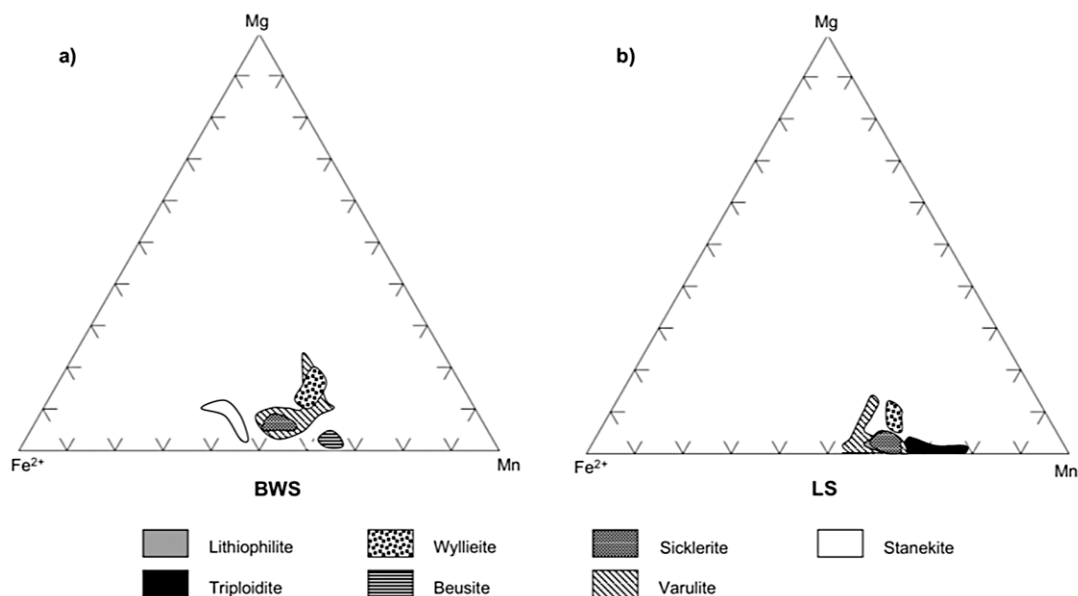
FIG. 4. Plots of the chemical composition of the primary and the early secondary phosphates from a) the beusite–wyllieite–sicklerite association (BWS) and, b) the lithiophilite–sicklerite association (LS).

TABLE 4. CHEMICAL COMPOSITION* OF THE MAIN PHOSPHATES FROM TWO ASSOCIATIONS: THE LITHIOPHILITE–SICKLERITE ASSOCIATION (LS), AND THE BEUSITE– WYLLIEITE–SICKLERITE ASSOCIATION (BWS)

	Lph	Sk	Sk	Tp	Stk	Dcn	Beu	Hur
Association	LS	LS	BWS	LS	BWS	BWS	BWS	LS
n	22	16	23	11	19	5	7	39
P_2O_5 wt.%	44.70	45.50	46.50	31.35	32.08	39.97	40.84	40.21
Al_2O_3	0.01	0.01	0.01	0.01	0.01	2.21	0.01	0.02
Fe_2O_3	0.00	19.17	22.08	0.00	28.30	0.00	0.00	0.00
FeO	16.84	0.00	0.00	19.85	0.00	17.39	18.04	0.81
MnO	27.41	28.31	23.22	43.35	19.52	23.95	33.52	43.45
MgO	0.54	0.53	1.94	0.47	2.10	2.28	0.61	1.50
CaO	0.03	0.08	0.17	0.01	0.34	2.69	6.87	0.39
K_2O	0.01	0.01	0.03	0.00	0.10	1.52	0.01	0.01
Na_2O	0.17	0.54	1.36	0.03	0.39	4.98	0.05	0.03
Total	89.73	94.15	95.30	95.79	96.77	94.99	99.95	86.42
P apfu	1.000	1.000	1.000	1.000	1.000	12.000	4.000	4.000
Al	0.000	0.000	0.000	0.000	0.000	0.924	0.002	0.003
Fe^{3+}	0.000	0.375	0.422	0.000	0.784	0.000	0.000	0.000
Fe^{2+}	0.372	0.000	0.000	0.670	0.000	5.158	1.745	0.079
Mn	0.614	0.622	0.499	1.336	0.609	7.192	3.284	4.324
Mg	0.021	0.020	0.073	0.033	0.115	1.204	0.106	0.263
Ca	0.001	0.002	0.005	0.001	0.014	1.021	0.852	0.049
K	0.000	0.000	0.001	0.000	0.004	0.688	0.001	0.002
Na	0.009	0.027	0.067	0.000	0.028	3.426	0.010	0.006
Fe/(Fe + Mn)	0.38	0.38	0.46	0.33	0.56	0.42	0.35	0.02

* Data obtained with an electron microprobe. The data reported are an average result on n point analyses. The cation numbers are calculated on the basis of $1PO_4$ per formula unit for lithiophilite, sicklerite, triploidite, and staněkite, $12PO_4$ for dickinsonite-(KMnNa), and $4PO_4$ for beusite and hureaulite. Symbols used: Lph: lithiophilite, Sk: sicklerite, Tp: triploidite, Stk: staněkite, Dcn: dickinsonite-(KMnNa), Beu: beusite, Hur: hureaulite.

TABLE 5. CHEMICAL COMPOSITION* OF VARULITE FROM TWO ASSOCIATIONS: THE LITHIOPHILITE–SICKLERITE ASSOCIATION (LS), AND THE BEUSITE–WYLLIEITE–SICKLERITE ASSOCIATION (BWS)

Assoc.	LS	BWS			LS	BWS
n	48	23			48	23
K_2O wt.%	0.06	0.06	M2	Al apfu	0.006	0.003
Na_2O	9.52	7.91		Fe^{3+}	4.605	5.335
CaO	0.76	0.53		Fe^{2+}	0.160	0.000
MgO	0.52	1.73		Mg	0.255	0.825
Al_2O_3	0.02	0.01		Mn	2.975	1.837
P_2O_5	43.02	44.24		ΣM2	8.000	8.000
MnO	26.33	22.51				
FeO	17.29	19.91	M1	Mn	4.000	4.000
				ΣM1	4.000	4.000
Total	97.53	96.90				
			A1	Mn	0.373	0.272
				Ca	0.268	0.183
				Na	3.359	3.545
				ΣA1	4.000	4.000
			A2´	Na	2.721	1.366
				K	0.027	0.023
				□	1.252	2.612
			Fe/(Fe + Mn)		0.39	0.47

* Data obtained with an electron microprobe. The data reported are an average result on n point analyses. The cation numbers are calculated on the basis of $12PO_4$ per formula unit. The cation positions are labeled according to the conventions of Hatert et al. (2000).

up to 3.5 cm long, that do not display a preferential orientation. These tourmaline crystals are in contact with the garnet crystals, or with garnet and muscovite. More rarely, they appear surrounded by a quartz crown. Occasionally, tourmaline crystals appear inside the K-feldspar, with a very fine layer of muscovite at the interface. Under the microscope, the tourmaline crystals generally show a concentric chromatic zoning, with bluish to grayish colors, commonly darker at the rim than in the core of the prisms.

Tourmaline structural formulae have been normalized to 31 anions (O, OH, F) using the Excel file provided by Selway & Xiong (www.open.ac.uk) (Table 8). The amount of B_2O_3 corresponding to three boron cations was constrained in the structural formula, as was the amount of H_2O. Tourmaline compositions have been recast into end-member components according to the scheme of Pesquera $et\ al.$ (2008). The tourmaline is quite homogeneous in composition in the investigated samples: all samples correspond to alkali tourmalines according to the nomenclature of Henry $et\ al.$ (2011) (Table 8, Fig. 6a), with schorl as main component in all crystals (35–41%), and with important amounts of the dravitic component (21–29%), and lower contents of foitite (11–21%) and magnesiofoitite (8–14%) (Table 8, Fig. 6b).

Twenty points have been analyzed across one of the tourmaline prisms in order to establish the behavior of the major elements during the crystallization of this mineral phase. However, no zonation was observed for any of the elements. Only the rim of this crystal shows a slight increase and decrease in Fe and Mg, respectively. Chemical variations observed in tourmaline from the Cema pegmatite seem to follow mainly the alkali-deficiency exchange-vector $Al^X\square\ (R^{2+}Na)_{-1}$, where $^X\square$ represents the vacancies at the X site; although the proton-loss mechanism $[AlO(R^{2+}(OH))_{-1}]$ was also operative, according to the plot of Al $versus$ Na (Fig. 6c).

The chemical composition of garnet ($Sps_{57}Alm_{41}$ Prp_2) is quite homogeneous and corresponds to a spessartine with an important almandine content (Table 9, Fig. 7).

DISCUSSION

The ratio Fe/(Fe + Mn)

There have been numerous studies on phosphate minerals in the literature ($e.g.,$ Fransolet $et\ al.$ 1986, Keller 1991, Keller & von Knorring 1989, Roda et $al.$ 1996, 1998, Černý $et\ al.$ 1998, Smeds $et\ al.$ 1998, Masau $et\ al.$ 2000, Guastoni $et\ al.$ 2007, Vignola $et\ al.$ 2008, Galliski $et\ al.$ 2009), but most of these investigations are mainly descriptive, the authors focusing their attention on paragenetic and compositional questions. References to the petrogenetic role of phosphates during the evolution of the pegmatites are scarce ($e.g.,$ London $et\ al.$ 1999, Roda $et\ al.$ 2004). On the other hand, the chemical composition of phosphates has been used frequently to establish the degree of evolution of

TABLE 6. CHEMICAL COMPOSITION* OF WYLLIEITE
FROM TWO ASSOCIATIONS,
THE LITHIOPHILITE–SICKLERITE ASSOCIATION (LS)
AND THE BEUSITE–WYLLIEITE–SICKLERITE ASSOCIATION (BWS)

Assoc	LS	BWS			LS	BWS
n	14	8			14	8
K_2O wt.%	0.01	0.02	M(2b)	Mg $apfu$	0.917	1.746
CaO	0.26	0.74		Fe^{2+}	3.083	1.823
P_2O_5	40.42	45.19		Mn	0.000	0.431
MnO	24.88	24.14		ΣM(2b)	4.000	4.000
FeO	13.51	14.67				
Na_2O	6.75	6.17	M(2a)	Al	1.907	1.899
Al_2O_3	4.61	5.14		Fe^{3+}	0.878	2.026
MgO	1.84	3.74		Mg	0.042	0.000
				Mn	1.173	0.075
Total	92.27	99.80		ΣM(2a)	4.000	4.000
			M(1)	Mn	4.000	4.000
				ΣM(1)	4.000	4.000
			X(1)	Na	1.688	1.843
				Ca	0.096	0.249
				Mn	2.216	1.908
				K	0.000	0.000
				$\square$	0.000	0.000
				ΣX(1)	4.000	4.000
			X(2)	Na	2.900	1.910
				$\square$	1.100	2.090
				ΣX(2)	4.000	4.000
				Fe/(Fe + Mn)	0.35	0.38

* Data obtained with an electron microprobe. The data reported are an average result on n point analyses. The cation numbers are calculated on the basis of $3PO_4$ per formula unit.

TABLE 7. CHEMICAL COMPOSITION* OF JAHNSITE-(CaMnMg)
FROM THE LITHIOPHILITE–SICKLERITE ASSOCIATION

K_2O wt.%	0.01	T	P $apfu$	4.488
CaO	5.49			
P_2O_5	38.06	M(3)	Fe^{2+}	1.954
MnO	11.17		Al	0.018
FeO	18.68		Mn	0.028
Na_2O	0.24		ΣM(3)	2.000
Al_2O_3	0.22			
MgO	7.25	M(2)	Mg	1.506
			Mn	0.494
Total	81.12		ΣM(2)	2.000
		M(1)	Mn	0.734
			Ca	0.266
			ΣM(1)	1.000
		X	Ca	0.624
			Na	0.053
			ΣX	0.677
			Fe/(Fe + Mn)	0.61

* Data obtained with an electron microprobe. These data represent an average result of six analyses. The cation numbers are calculated on the basis of 24 atoms of oxygen per formula unit.
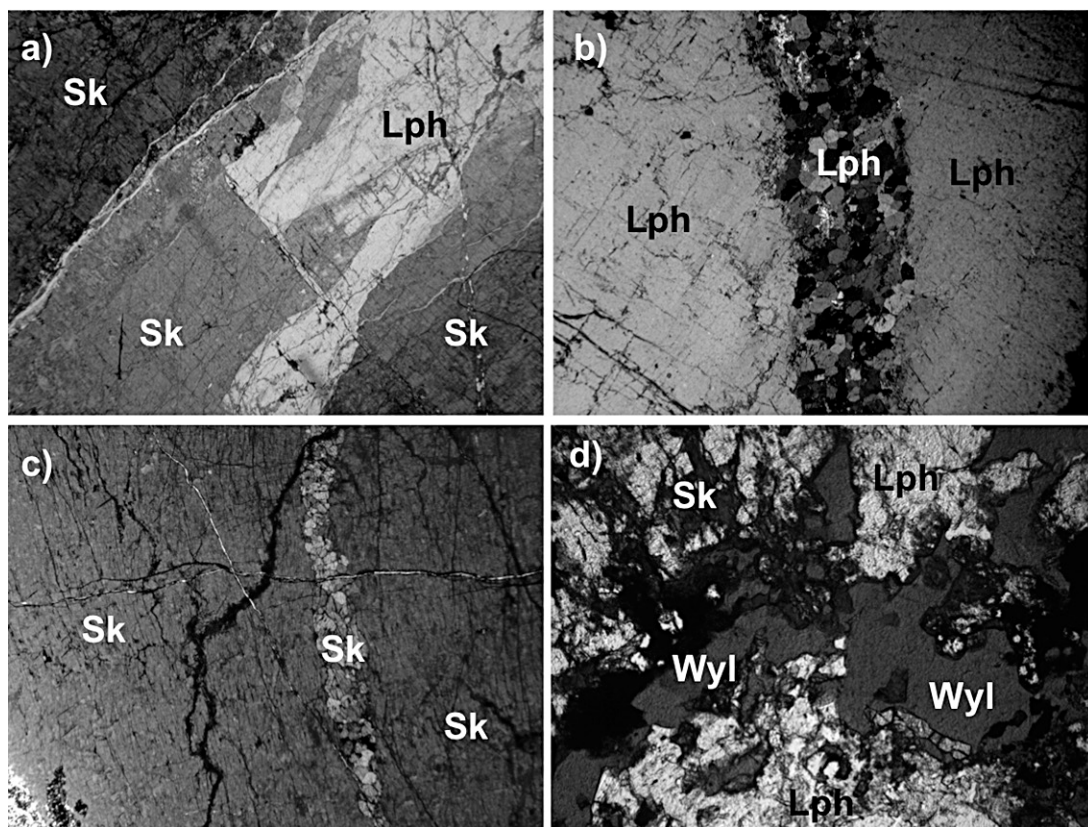
FIG. 5.   Photomicrographs of the main textures observed in the LS association from the Cema pegmatite (all plane-polarized light except b). a) Replacement of lithiophilite by sicklerite, with a gradual change in color in some areas. b) Very fine-grained elongate zone of granular texture of lithiophilite, inside medium-grained lithiophilite crystals. c) Same as b) for sicklerite. d) Interstitial crystals of wyllieite inside lithiophilite, which is partially replaced by orange sicklerite. Symbols: Lph: lithiophilite, Sk: sicklerite, Wyl: wyllieite.

their host pegmatites, just as the composition of some silicates (micas, K-feldspar, tourmaline and beryl) and of oxides (columbite-group minerals) has been used. Indeed, a decrease of the Fe/(Fe + Mn) value has commonly been reported in phosphates, associated with increasing evolution of pegmatites (Ginsburg 1960, Fransolet *et al.* 1986, Keller 1994, Keller *et al.* 1994, Roda *et al.* 2005, Roda-Robles *et al.* 2010). In the most differentiated pegmatites, the phosphates are expected to be richer in Mn than in Fe.

Taking into account the mineralogy and the composition of the various phases, the Cema pegmatitic body may be grouped in the spodumene subtype of complex type, REL–Li subclass, in the classification scheme of Černý & Ercit (2005), being intermediate between moderately and highly evolved. Phosphates from the two associations, BWS and LS, occurring in the Cema pegmatite show different Fe/(Fe + Mn) values, but

in every case less than 0.5 in the primary and early secondary phases. Keeping in mind that the lowest Fe/(Fe + Mn) values in phosphates are supposed to be associated with the highest degrees of pegmatitic evolution, these values of Fe/(Fe + Mn) in the Cema phosphates are relatively low, considering the mineralogy of the whole pegmatite. In the Cema pegmatite, the Fe/(Fe + Mn) value thus does not reflect directly the degree of evolution attained by this pegmatitic body. In order to explain the relative abundance of Mn in relation to Fe in the early phosphates from Cema, it is necessary to take into account the other Fe–Mn–(Mg)-rich phases occurring in the pegmatite: tourmaline and garnet. Tourmaline (Mg-rich schorl) is quite abundant in the border and wall zones of the pegmatite, constituting approximately 8% in volume of these zones. Garnet (Fe-rich spessartine) is less abundant, close to 1% in volume. Therefore, Fe–Mn–(Mg)-rich silicates and phosphates occur in

this pegmatite. However, they have not been found in close contact: no skeletal or graphic intergrowths have been observed between these two groups of minerals, whereas these intergrowths are reported for other occurrences of mafic silicates and phosphates (*e.g.*, London *et al.* 1999, Alfonso & Melgarejo 2000, Roda *et al.* 2004). In the Cema pegmatite, it seems that the crystallization of mafic silicates and phosphates was not simultaneous,

but sequential, as proposed by London *et al.* (1999) as a general rule for pegmatites where these two groups of minerals appear. Galliski *et al.* (2009) interpreted similarly the association of beusite, lithiophilite and qingheiite in the Santa Ana pegmatite, also in San Luis Province. Therefore, we propose that during an inward crystallization from the margins, the formation of Fe–(Mg)-rich tourmaline (Fig. 7) in the border and

TABLE 8. REPRESENTATIVE COMPOSITIONS* OF TOURMALINE
FROM THE BORDER AND WALL ZONES OF THE CEMA PEGMATITE

Sample		p1	p2	p4	p6	p9	p14	p11	p12	p13	p16	p18	p19
SiO_2 wt.%		36.66	36.28	36.41	36.65	36.14	36.71	36.22	36.21	36.26	36.47	36.21	36.49
TiO_2		0.00	0.09	0.06	0.07	0.00	0.05	0.04	0.17	0.23	0.01	0.11	0.00
Al_2O_3		33.37	32.94	33.00	32.91	33.06	33.18	32.58	32.49	33.35	33.60	33.51	33.83
Cr_2O_3		0.07	0.00	0.09	0.02	0.05	0.01	0.00	0.02	0.00	0.10	0.00	0.00
FeO		10.30	10.28	10.64	10.46	10.56	10.,6	10.72	11.11	10.27	10.58	10.66	10.43
MgO		3.69	4.37	4.21	4.24	4.03	3.79	4.24	4.26	3.87	3.92	4.00	3.87
CaO		0.10	0.15	0.12	0.16	0.13	0.08	0.13	0.18	0.08	0.10	0.12	0.10
MnO		0.26	0.28	0.21	0.22	0.27	0.31	0.30	0.16	0.24	0.25	0.05	0.35
ZnO		0.31	0.35	0.25	0.11	0.00	0.15	0.21	0.21	0.08	0.17	0.10	0.01
Na_2O		2.00	2.40	2.08	2.35	2.16	1.98	2.18	2.17	1.92	2.11	2.11	2.16
K_2O		0.02	0.05	0.01	0.05	0.04	0.06	0.00	0.03	0.03	0.02	0.03	0.02
F		0.12	0.00	0.48	0.32	0.80	0.28	0.25	0.39	0.28	0.05	0.32	0.12
H_2O**		3.59	3.65	3.42	3.51	3.25	3.51	3.50	3.45	3.50	3.64	3.50	3.61
B_2O_3**		10.57	10.58	10.57	10.60	10.51	10.54	10.50	10.53	10.53	10.62	10.57	10.63
Total		101.05	101.43	101.56	101.66	100.98	100.71	100.88	101.37	100.64	101.65	101.29	101.62
O=F		0.05	0.00	0.20	0.13	0.34	0.12	0.11	0.16	0.12	0.02	0.13	0.05
Total**		101.00	101.43	101.36	101.53	100.65	100.59	100.77	101.20	100.53	101.63	101.16	101.57
T	Si *apfu*	6.028	5.963	5.985	6.009	5.978	6.050	5.994	5.979	5.986	5.970	5.953	5.968
	Al	0.000	0.037	0.015	0.000	0.022	0.000	0.006	0.021	0.014	0.030	0.047	0.032
	B	3.000	3.000	3.000	3.000	3.000	3.000	3.000	3.000	3.000	3.000	3.000	3.000
Z	Al	6.000	6.000	6.000	6.000	6.000	6.000	6.000	6.000	6.000	6.000	6.000	6.000
Y	Al	0.466	0.343	0.378	0.360	0.424	0.446	0.349	0.303	0.475	0.451	0.446	0.488
	Ti	0.000	0.012	0.008	0.009	0.000	0.007	0.005	0.021	0.029	0.001	0.014	0.000
	Cr	0.008	0.000	0.012	0.002	0.006	0.001	0.000	0.002	0.000	0.013	0.000	0.000
	Mg	0.903	1.072	1.031	1.035	0.995	0.932	1.046	1.047	0.951	0.957	0.982	0.945
	Mn	0.036	0.039	0.029	0.031	0.038	0.043	0.042	0.022	0.034	0.035	0.007	0.048
	Fe^{2+}	1.416	1.413	1.462	1.434	1.460	1.386	1.484	1.534	1.418	1.449	1.465	1.427
	Zn	0.037	0.043	0.030	0.013	0.000	0.018	0.026	0.026	0.010	0.021	0.012	0.001
	ΣY	2.867	2.921	2.950	2.885	2.923	2.833	2.951	2.954	2.916	2.927	2.926	2.909
X	Ca	0.018	0.026	0.027	0.028	0.022	0.014	0.023	0.032	0.015	0.018	0.020	0.018
	Na	0.638	0.742	0.765	0.746	0.692	0.632	0.700	0.696	0.614	0.671	0.672	0.685
	K	0.005	0.005	0.010	0.010	0.008	0.012	0.001	0.007	0.007	0.004	0.007	0.005
	□	0.339	0.228	0.197	0.215	0.278	0.341	0.277	0.266	0.365	0.308	0.300	0.292
	OH	3.940	3.929	4.000	3.834	3.583	3.856	3.868	3.798	3.856	3.976	3.834	3.941
	F	0.060	0.071	0.000	0.166	0.417	0.144	0.132	0.202	0.144	0.024	0.166	0.059
Schorl %		36	41	40	41	38	34	39	40	34	36	37	3
Dravite		22	27	29	28	25	22	27	26	22	23	24	2
Olenite		5	6	7	6	6	5	3	3	5	7	7	8
Foitite		20	13	11	12	16	21	16	16	21	18	18	17
Magnesiofoitite		13	9	8	9	11	14	11	11	14	12	12	11
others		4	4	5	4	4	4	4	4	4	4	2	5

* Data obtained with an electron microprobe. The structural formula is calculated on the basis of 31 anions.
** Amount inferred from considerations of stoichiometry.

wall zones, prior to the crystallization of phosphates in the outer core, could have depleted significantly the concentration in Fe in the pegmatite-forming melt, where the primary concentration of transition-metal cations usually is low, as suggested for peraluminous granitic melts by Puziewicz & Johannes (1988, 1990). Consequently, the primary growth of schorl seems to have strongly influenced the composition of phosphates in the Cema body, favoring relatively low Fe/(Fe + Mn) values, compared to the degree of evolution of the hosting pegmatite. A similar influence of the early crystallization of mafic silicates on the Fe/(Fe + Mn) values in phosphates was reported by London & Burt (1982) and London (2008) for the White Picacho District, in Arizona. It is noteworthy that spessartine-rich garnet coexists with the Fe-rich tourmaline in the border and wall zones of Cema. The differences in Fe/(Fe + Mn) for these two coexisting phases (Fig. 7) may be explained by the ability of tourmaline to control this ratio (London *et al*. 2001), Fe being more compatible than Mn in this mineral (Wolf & London 1997), whereas garnet shows a clear preference for Mn (London 2008). Spessartine-rich garnet became unstable as phosphorus contents increased in the melt. When this melt attained intermediate degrees of evolution, Mn-rich phosphates started crystallizing in the outer core zone of the pegmatite, succeeding garnet, as proposed by London *et al*. (1999) and London (2008).

On the other hand, in the LS association, most of the later secondary phases are, opposite to the early phases, richer in Fe than in Mn, with Fe/(Fe + Mn) values in the range 0.68–0.80 for rockbridgeite, 0.79–0.82 for phosphoferrite, 0.89–0.92 for lipscombite, 0.59–0.61 for tavorite, and 0.61 for jahnsite-(CaMnMg)
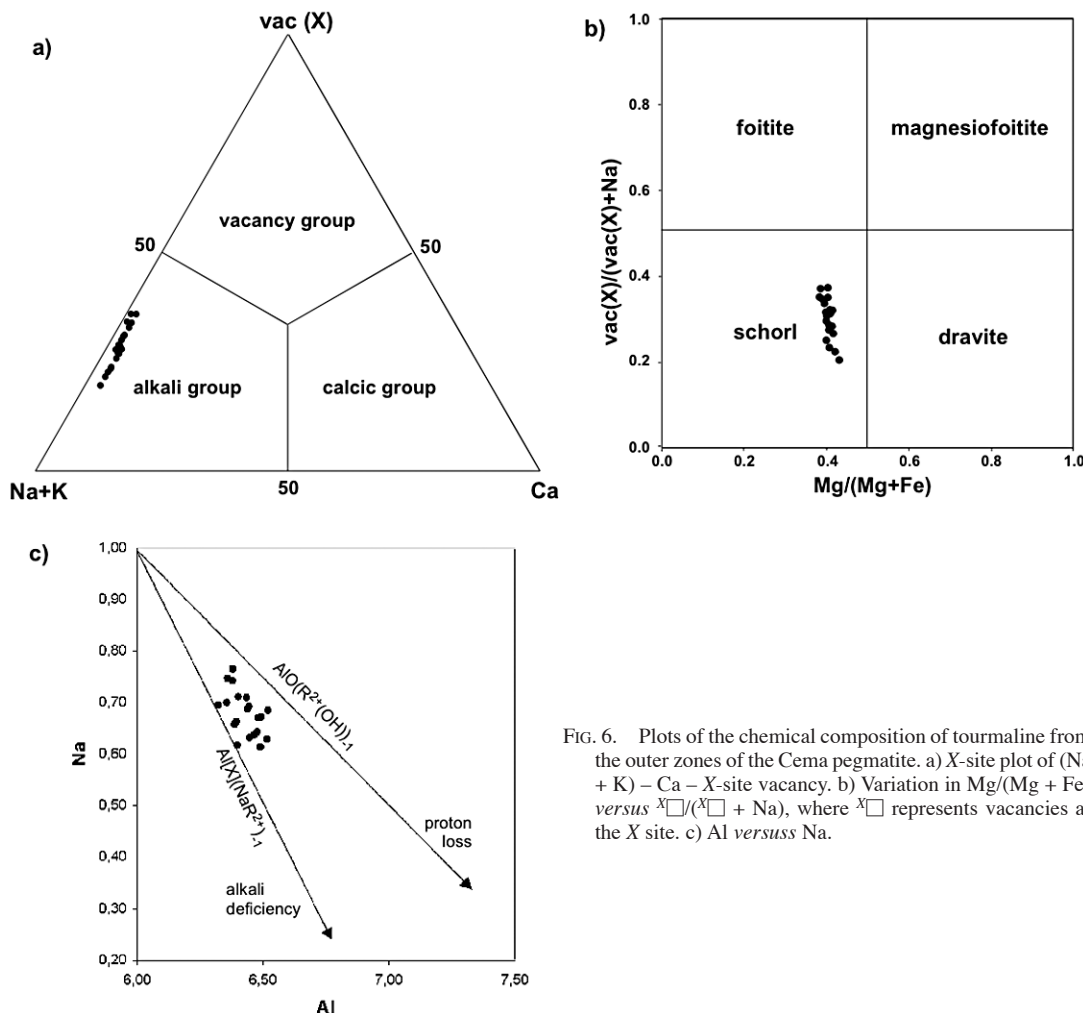

Fig. 6. Plots of the chemical composition of tourmaline from the outer zones of the Cema pegmatite. a) *X*-site plot of (Na + K) – Ca – *X*-site vacancy. b) Variation in Mg/(Mg + Fe) *versus* $^X\square/(^X\square + Na)$, where $^X\square$ represents vacancies at the *X* site. c) Al *versuss* Na.
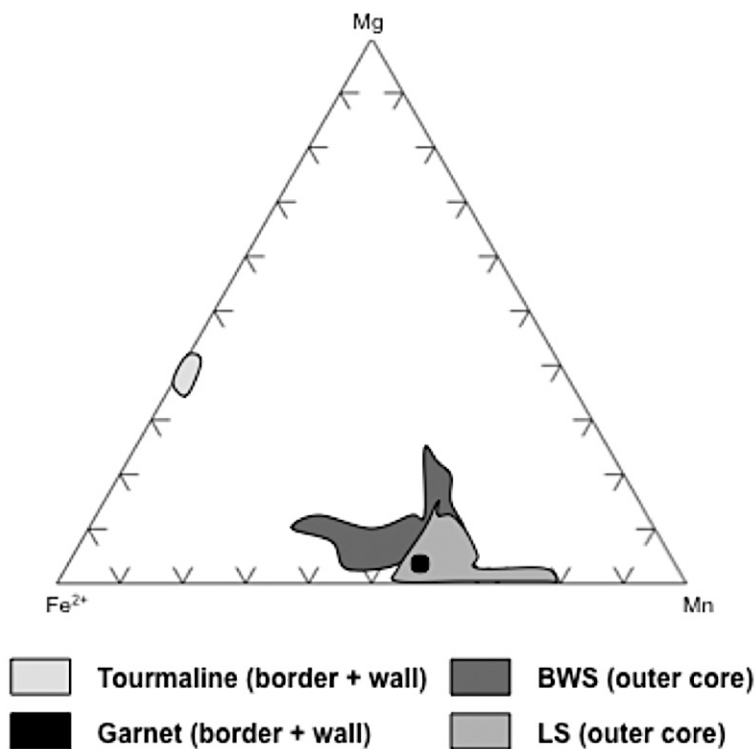
FIG. 7.   Plot of the variation in the contents in Mg, total Fe (as Fe^{2+}), and Mn for
tourmaline, garnet and phosphates from the Cema pegmatite.

(Table 7). This could be due to the preference of Mn to form oxides and hydroxides as temperature decreases, whereas Fe, mainly Fe^{3+}, enters preferently into phosphates during the low-temperature alteration stages, as suggested by Fransolet (2007).

Paragenetic and compositional relationships

Two different phosphate associations have been distinguished in this zone. The mineral paragenesis are different for both associations, as well as the Fe/(Fe + Mn) values and the Li and Mg contents. The LS association, rich in lithiophilite and sicklerite, shows lower values of Fe/(Fe + Mn) than the BWS, which is rich in sicklerite, beusite, and wyllieite. Therefore, we could consider that, even if occurring in the same zone, the BWS association crystallized first, when the Li activity in the pegmatite-forming melt was still low. At lower temperatures, and with higher Li activity in the melt, the LS association formed.

The Mg contents change also significantly for the early phosphate phases from the two associations, with lower Fe/(Fe + Mg) values in the BWS than in the LS

(Fig. 7) (*e.g.,* 0.85 *versus* 0.95 for sicklerite, 0.87 *versus* 0.93 for varulite and 0.69 *versus* 0.89 for wyllieite). This decrease in the Mg proportion in phosphates during pegmatitic crystallization is also observed in the Cañada pegmatite, in Salamanca, Spain (Roda *et al.* 2004), where phosphates and mafic silicates also occur together. In that case, a contamination from the country rock (gabbro) is assumed, as the Mg values are extremely high in the border zone, and they decrease dramatically inward. However, in the Cema pegmatite the two phosphates associations occur in the same zone (outer core). Moreover, in this case, the country rock (mica schists) is not Mg-rich, which runs against the idea of a contamination in Mg from outside the pegmatitic system. The fact that Mg contents are higher in the first-crystallized BWS association than in the later LS supports the idea that Mg is a primary component of the system that was not completely exhausted during the crystallization of tourmaline in the border and wall zones, and that was consumed later, mainly during the crystallization of the phosphates from the earlier BWS.

Alteration sequences deduced from the petrography and composition of the two phosphate associations are

proposed in Figure 8. It is noteworthy that varulite, the Mn-rich equivalent of alluaudite, was observed in the two associations. This early secondary phosphate has been generally considered as a product of a Na-metasomatic process (Fransolet *et al.* 1986, Keller & von Knorring 1989, Roda *et al.* 1996, 1998, 2004, Roda Robles *et al.* 2010). In our occurrence, an episode of albitization has been reported in the Cema pegmatite (Roquet 2010), with the development of some replacement bodies. Consequently, we can consider that varulite formed during this episode of Na metasomatism, at a subsolidus stage. Sicklerite is also a product of early replacement, in turn replaced by varulite in the BWS association.

The behavior of P

Although P generally occurs as a minor element in most aluminosilicate melts, it may have an important influence on some properties of the melt, such as the expansion of the liquidus field of quartz relative to that of feldspar (London *et al.* 1993), to reduce the liquidus temperatures (Tien & Hummel 1962, Wyllie & Tuttle 1964), to increase the polymerization of silicate tetrahedra (Kushiro 1975), or to promote the liquid immiscibility in silicate systems (Rutherford

TABLE 9. REPRESENTATIVE COMPOSITIONS* OF GARNET FROM THE BORDER AND WALL ZONES OF THE CEMA PEGMATITE

sample	p11	p13-1	p13-2	p13-3
SiO_2 wt.%	36.48	36.55	36.61	36.50
TiO_2	0.03	0.00	0.02	0.00
Al_2O_3	20.18	20.24	20.15	20.32
MgO	0.59	0.64	0.65	0.58
CaO	0.41	0.43	0.36	0.41
MnO	25.50	25.01	24.31	24.74
FeO	17.76	18.45	17.77	18.03
Na_2O	0.01	0.03	0.00	0.02
K_2O	0.01	0.01	0.00	0.00
Cr_2O_3	0.00	0.00	0.01	0.03
Total	100.97	101.36	99.87	100.64
Si *apfu*	3.000	3.000	3.000	3.000
Al	1.957	1.959	1.947	1.969
Ti	0.004	0.000	0.002	0.000
Cr	0.000	0.000	0.001	0.004
Fe^{2+}	2.443	2.532	2.436	2.479
Mn	3.552	3.478	3.375	3.445
Mg	0.144	0.156	0.159	0.143
Ca	0.073	0.075	0.063	0.072
Na	0.002	0.010	0.000	0.007
K	0.002	0.003	0.000	0.000
Fe/(Fe+Mg)	0.94	0.94	0.94	0.95
Fe/(Fe+Mn)	0.41	0.42	0.42	0.42
Fe/(Fe+Mg+Mn)	0.40	0.41	0.41	0.41
% FeO	39.80	41.06	40.80	40.85
% MnO	57.85	56.41	56.53	56.77
% MgO	2.35	2.53	2.67	2.36

* Data obtained with an electron microprobe.

et al. 1974), which could induce unusual magmatic processes (Visser & Koster van Groos 1979). According to Mysen & Richet (2005), the solution of P^{5+} in silica-rich melts is energetically unfavorable, the solubility of phosphorus in melts depending on silicate melt composition. The content of silica and alumina seems to have the strongest influence on this solubility. In the case of silica, Harrison & Watson (1984) proposed that, for natural melts, apatite solubility is a negative function of SiO_2 content, taking into account that the partition coefficient, $D^{apatite/melt}$ increases with increasing SiO_2 content. In the case of alumina, the effect is opposite, particularly in peraluminous silicate melts, where the P_2O_5 solubility increases rapidly with Al content (Bea *et al.* 1992, Wolf & London 1994). Phosphorus solubility in silicate melts seems to be also a positive function of temperature (Harrison & Watson 1984, Mysen & Richet 2005), whereas during the final stages of crystallization in a H_2O-saturated granitic melt, according to Keppler (1994), the behavior of phosphorus is controlled by the emplacement depth of the pluton. Therefore, the role of phosphorus during crystallization of relatively P-rich melts, such as many pegmatite-forming melts, may become important, and its behavior difficult to establish, as it depends on several factors. In the case of the Cema pegmatite, phosphates occurring in the outer core zone indicate that P behaved as an incompatible element until the intermediate stages of pegmatitic crystallization, when saturation in phosphates was attained, as is reported in other phosphate-bearing pegmatites (Roda *et al.* 1998, 2004, 2005). The rounded shape of some of the nodules where these phosphates occur, as well as the bulk composition of these masses, where more than 99% by weight belongs to phosphate minerals, could suggest that these phosphates crystallized from a P-rich melt segregated from a volumetrically much more important silicate-rich melt. Rutherford *et al.* (1974) suggested that enrichment in phosphorus in late-stage magmas may result in liquid immiscibility. Previously, James & McMillan (1970) have shown evidence for such immiscibility in quenched liquids in the system $Li_2O–SiO_2–P_2O_5$. However, according to the experimental study of phosphate crystallization from hydrous aluminosilicate melts by Shigley & Brown (1986), any silicate–phosphate liquid immiscibility seems to be ruled out. In addition to this controversy, in case it was possible that a silicate magma reached saturation in a phosphate melt, the concentration of P needed to attain this point is presumably far from the concentrations in P proposed for the pegmatite-forming melts, usually in the order of 1–3 wt% (London 1992, 2008, London *et al.* 1999, Breiter & Köller 2001, Roda *et al.* 2004, 2005). However, Thomas & Webster (2000) described inclusions in quartz that contain ~22 wt% P_2O_5, whereas Veksler *et al.* (2003) recognized berlinite inclusions in quartz from pegmatites. London (2008) interpreted these unusual high concentrations of P as evidence of boundary-layer melts, that is, a part of
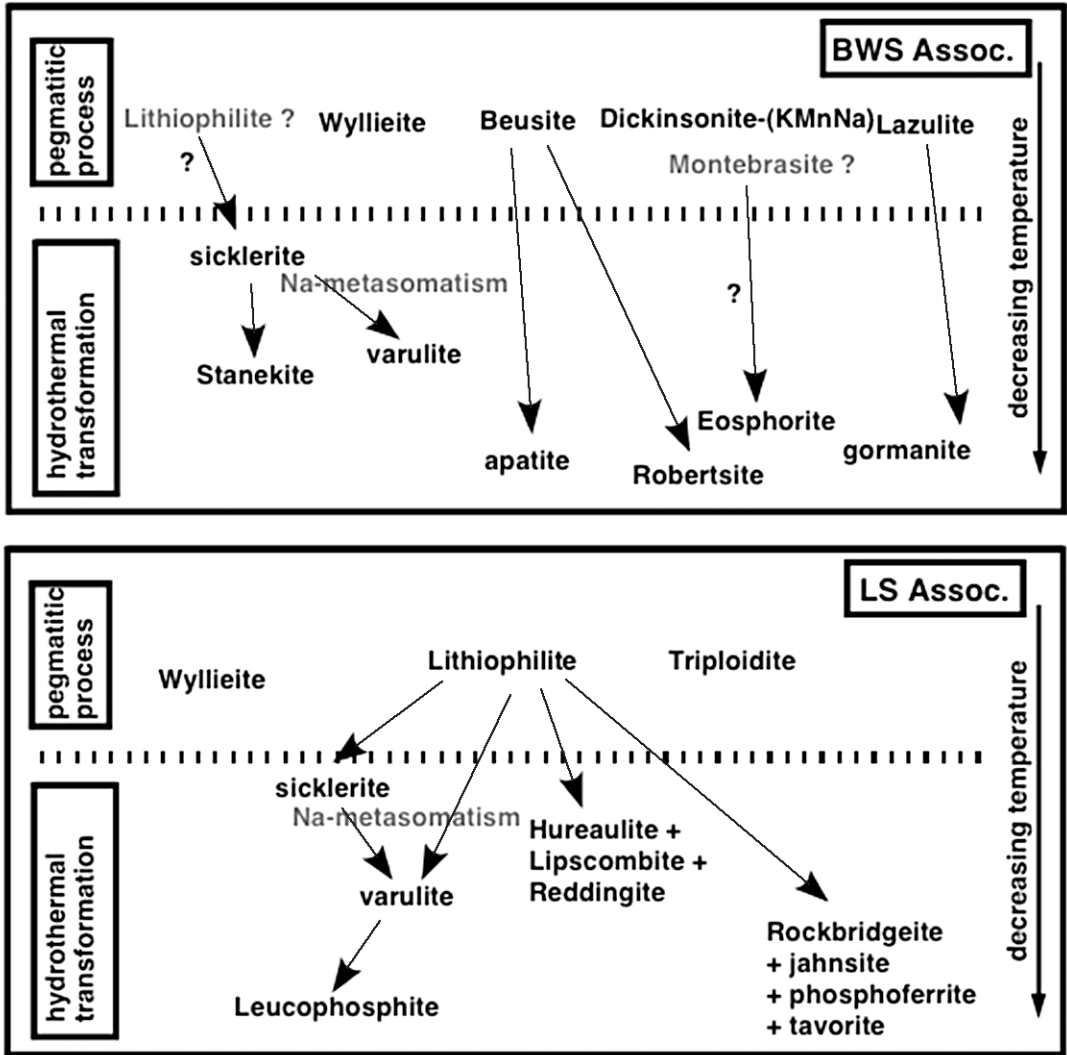
FIG. 8.	Diagram showing alteration sequences of phosphate minerals from the two associations.

the melt where the incompatible elements concentrate during the crystallization of the pegmatite-forming melt. This way, it would not represent the whole composition of the melt, but the composition of a reduced volume of the melt during a certain moment in the crystallization of the pegmatite. Rounded to ellipsoidal nodules of phosphates are common not only in the Cema pegmatite, but they are the most frequent shape for the occurrence of phosphates in many phosphate-bearing pegmatites. It is also common that these nodules are located in the outer core zone or core margin of these bodies. If we take into account that after the crystal-

lization of these zones, the main mineral to crystallize is quartz, whereas in the intermediate zones, feldspars and other Al-bearing silicates are abundant; the silicate melt must be relatively enriched in silica and depleted in alumina during the crystallization of these phosphates nodules. This, together with a decrease in the temperature as crystallization proceeds, would favor the immiscibility of phosphate in the silicate melt. Whether at this point the melt presented an enrichment due to a process of constitutional zone refining or by other process of crystal fractionation is not easy to ascertain from the available data. What is clear is that in the Cema

pegmatite, an inward crystallization from the border to the core was developed. During this crystallization, the phosphorus behaved as an incompatible element until the intermediate stages, when saturation in phosphates was attained. Whether the increase in the phosphorus concentration of the silicate melt was high enough to reach saturation in a phosphate melt or not is difficult to say at the present level of knowledge, but the shape and composition of the phosphate nodules from the Cema pegmatite do not allow the rejection of such a possibility. The occurrence of two different phosphate associations, with different Fe/(Fe + Mn) values and Mg and Li contents, suggests that, if such P-rich melt segregated, it also presented a fractionation, with an enrichment in Mn and Li and a decrease in Mg as crystallization proceeded.

Conclusions

The following conclusions are drawn, regarding the formation of the Cema pegmatite:

1) Iron–Mn phosphates nodule are common at the outer core zone of the Cema pegmatite.

2) Two different complex phosphate associations have been distinguished: a) beusite–wyllieite– sicklerite-rich (BWS), and b) lithiophilite–sicklerite-rich (LS).

3) Sicklerite, varulite and hureaulite are the main early secondary products in the LS association, whereas in the BWS association, sicklerite, varulite, and staněkite are the main early secondary phases.

4) According to the mineralogical and chemical data, a higher temperature of crystallization is proposed for the BWS association than for the LS association.

5) The important Mn enrichment observed in the early phosphates from the Cema body, which is not a highly fractionated pegmatite, can be explained as a result of the previous crystallization of schorl in the border and wall zones of this pegmatite, which strongly depleted the activity of Fe in the remaining pegmatite-forming melt.

6) The crystallization of Mn-rich phosphates at the outer core zone of the pegmatite took place at an intermediate degree of evolution, when the pegmatite-forming melt became saturated in phosphates, the formation of an immiscible P-rich melt being both difficult to ascertain and to reject definitely.

References

Alfonso, P. & Melgarejo, J.C. (2000): Boron *vs.* phosphorus in granitic pegmatites: the Cap the Creus case (Catalonia, Spain). *J. Czech Geol. Soc.* **45**(1-2), 131-141.

Bea, F., Fershater, G. & Corretgé, L.G. (1992): The geochemistry of phosphorus in granite rocks and the effect of aluminium. *Lithos* **29**, 43-56.

Boury, P. (1981): *Comportement du fer et du manganèse dans les associations de phosphates pegmatitiques*. Thèse de maîtrise, Université de Liège, Liège, Belgique.

Breiter, K. & Köller, F. (2001): Mineralogy of extremely fractionated phosphorus-rich granite: Podlesí, Czech Republic. *Mitt. Österreich. Mineral. Gesells.* **146**, 37-39.

Černý, P. & Ercit, T.S. (2005): The classification of granitic pegmatites revisited. *Can. Mineral.* **43**, 2005-2026.

Černý, P., Selway, J.B., Ercit, T.S., Breaks, F.W., Anderson, A.J. & Anderson, S.D. (1998): Graftonite–beusite in granitic pegmatites of the Superior Province: a study in contrasts. *Can. Mineral.* **36**, 367-376.

Fransolet, A.-M. (2007): Phosphate associations in the granitic pegmatites: the relevant significance of these accessory minerals. *In* Granitic Pegmatites: the State of the Art. Universidade do Porto, Departamento de Geología, Memorias **8**, 7-8.

Fransolet, A.-M., Abraham, K. & Speetjens, J.-M. (1985): Evolution génétique et signification des associations de phosphates de la pegmatite d'Angarf-Sud, plaine de Tazenakht, Anti-Atlas, Maroc. *Bull. Minéral.* **108**, 551-574.

Fransolet, A.-M., Keller, P. & Fontan, F. (1986): The phosphate mineral associations of the Tsaobismund pegmatite, Namibia. *Contrib. Mineral. Petrol.* **92**, 502-517.

Galliski, M.A. (1994): La Provincia Pegmatítica Pampeana. I. Tipología y distribución de sus distritos económicos. *Revista Asociación Geológica Argentina* **49**, 99-112.

Galliski, M.A. (2009): The Pampean pegmatite province, Argentina: a review. *In* Contrib. 4th Int. Symp. Granitic Pegmatites, PEG2009 BRAZIL. *Estudos Geológicos* **19**(2), 30-34.

Galliski, M.A., Oyárzabal, J.C., Márquez-Zavalía, M.F. & Chapman, R. (2009): The association qingheiite–beusite–lithiophilite in the Santa Ana pegmatite, San Luis, Argentina. *Can. Mineral.* **47**, 1213-1223.

GINSBURG, A.I. (1960): Specific geochemical features of the pegmatitic process. *21st Int. Geol. Congress* (*Norden*) **17**, 111-121.

GUASTONI, A., NESTOLA, F., MAZZOLENI, G. & VIGNOLA, P. (2007): Mn-rich graftonite, ferrisicklerite, staněkite and Mn-rich vivianite in a granitic pegmatite at Soe' Valley, central Alps, Italy. *Mineral. Mag.* **71**, 579-585.

HARRISON, T.M. & WATSON, E.B. (1984): The behavior of apatite during crustal anatexis: equilibrium and kinetic considerations. *Geochim. Cosmochim. Acta* **48**, 1468-1477.

HATERT, F., KELLER, P., LISSNER, F., ANTELUCCI, D. & FRANSOLET, A.-M. (2000): First experimental evidence of alluaudite-like phosphates with high Li-content: the $(Na_{1-x}Li_x)MnFe_2(PO_4)_3$ series (x = 0 to 1). *Eur. J. Mineral.* **12**, 847-857.

HENRY, D., NOVÁK, M., HAWTHORNE, F.C., ERTL, A., DUTROW, B., UHER, P. & PEZZOTTA, F. (2011): Nomenclature of the tourmaline supergroup-minerals. *Am. Mineral.* **96**, 895-913.

HURLBUT, C.S., JR. & ARISTARAIN, L.F. (1968): Beusite, a new mineral from Argentina, and the graftonite–beusite series. *Am. Mineral.* **53**, 1799-1814.

HUVELIN, P., ORLIAC, M. & PERMINGEAT, F. (1972): Ferri-alluaudite calcifère de Sidi-bou-Othmane (Jebilet, Maroc). *Notes du Service géologique du Maroc* **32**, 241, 35-49.

JAMES, P.F. & MCMILLAN, P.W. (1970): Quantitative measurements of phase separation in glasses using transmission electron microscopy. 2. A study of lithia-silica glasses and the influence of phosphorus pentoxide. *Phys. Chem. Glasses* **1**(1), 64-70.

KELLER, P. (1991): The occurrence of Li–Fe–Mn phosphate minerals in granitic pegmatites of Namibia. *Commun. Geological Survey of Namibia* **7**, 21-34.

KELLER, P. (1994): The mineralogical and geochemical role of Fe–Mn-phosphate minerals in the evolutionary process of granitic pegmatites – new results from Namibia. *Int. Mineral. Assoc.*, *16th, Gen. Meeting* (*Pisa*), *Abstr.*, 198.

KELLER, P., FONTAN, F. & FRANSOLET, A.-M. (1994): Intercrystalline cation partitioning between minerals of the triplite–zwieselite–magniotriplite and the triphylite–lithiophilite series in granitic pegmatites. *Contrib. Mineral. Petrol.* **118**, 239-248.

KELLER, P. & VON KNORRING, O. (1989): Pegmatites at the Okatjimukuju farm, Karibib, Namibia. I. Phosphate mineral associations of the Clementine II pegmatite. *Eur. J. Mineral.* **1**, 567-593.

KEPPLER, H. (1994): Partitioning of phosphorus between melt and fluid in the system haplogranite–H_2O–P_2O_5. *Chem. Geol.* **117**, 345-353.

KUSHIRO, I. (1975): On the nature of silicate melt and its significance in magma genesis: regularities in the shift of liquidus boundaries involving olivine, pyroxene, and silica materials. *Am. J. Sci.* **275**, 411-431.

LONDON, D. (1992): Phosphorus in S-type magmas: the P_2O_5 content of feldspars from granites, pegmatites, and rhyolites. *Am. Mineral.* **77**, 126-145.

LONDON, D. (2008): *Pegmatites*. The Canadian Mineralogist, Special Publication 10.

LONDON, D. & BURT, D.M. (1982): Alteration of spodumene, montebrasite and lithiophilite in pegmatites of the White Picacho District, Arizona. *Am. Mineral.* **67**, 494-509.

LONDON, D., EVENSEN, J.M., FRITZ, E., ICENHOWER, J.P., MORGAN, G.B., VI & WOLF, M.B. (2001): Enrichment and accommodation of manganese in granite–pegmatite systems. *11th Annual Goldschmidt Conference*, Abstract **3369**, *Lunar Planetary Institute, Contrib.* **1088** (CD-ROM).

LONDON, D., MORGAN, G.B., VI, BABB, H.A. & LOOMIS, J.L. (1993): Behavior and effects of phosphorus in the system Na_2O–K_2O–Al_2O_3–SiO_2–P_2O_5–H_2O at 200 MPa (H_2O). *Contrib. Mineral. Petrol.* **113**, 450-465.

LONDON, D., WOLF, M.B., MORGAN G.B., VI & GALLEGO GARRIDO, M. (1999): Experimental silicate–phosphate equilibria in peraluminous granitic magmas, with a case study of the Alburquerque batholith at Tres Arroyos, Badajoz, Spain. *J. Petrol.* **40**, 215-240.

MASAU, M., STANĚK, J., ČERNÝ, P. & CHAPMAN, R. (2000): Metasomatic wolfeite and associated phosphates from the Otov I granitic pegmatite, western Bohemia. *J. Czech Geol. Soc.* **45**(1–2), 159-173.

MYSEN, B. & RICHET, P. (2005): *Silicate Glasses and Melts: Properties and Structure*. Elsevier, Amsterdam, The Netherlands.

OYARZÁBAL, J.C. & GALLISKI, M.-A. (2007): Huréaulita $Mn^{2+}_5(H_2O)_4[PO_3(OH)]_2[PO_4]_2$, de diferentes yacimientos del distrito pegmatítico Totoral, San Luis, Argentina. *Revista Asociación Geológica Argentina* **62**(2), 210-216.

PESQUERA, A., TORRES, F., GIL-CRESPO, P. & TORRES-RUIZ, J. (2008): TOURCOMP: a program for estimating end-member proportions in tourmalines. *Mineral. Mag.* **72**, 1021-1034.

PUZIEWICZ, J. & JOHANNES, W. (1988): Phase equilibria and compositions of Fe–Mg–Al minerals and melts in water-saturated peraluminous granitic systems. *Contrib. Mineral. Petrol.* **100**, 156-168.

PUZIEWICZ, J. & JOHANNES, W. (1990): Experimental study of a biotite-bearing granitic system under water-saturated and water-undersaturated conditions. *Contrib. Mineral. Petrol.* **104**, 397-406.

RODA, E., FONTAN, F., PESQUERA, A. & KELLER, P. (1998): The Fe–Mn phosphate associations from the Pinilla de Fermoselle pegmatite, Zamora, Spain: occurrence of kryzhanovskite and natrodufrénite. *Eur. J. Mineral.* **10**, 155-167.

RODA, E., FONTAN, F., PESQUERA, A. & VELASCO, F. (1996): The phosphate mineral association of the granitic pegmatites of the Fregeneda area (Salamanca, Spain). *Mineral. Mag.* **60**, 767-778.

RODA, E., PESQUERA, A., FONTAN, F. & KELLER, P. (2004): Phosphate mineral associations in the Cañada pegmatite (Salamanca, Spain): paragenetic relationships, chemical compositions, and implications for pegmatite evolution. *Am. Mineral.* **89**, 110-125.

RODA, E., PESQUERA, A, GIL-CRESPO, P.P., TORRES-RUIZ, J. & FONTAN, F. (2005): Origin and internal evolution of the Li–F–Be–B–P-bearing Pinilla de Fermoselle pegmatite (Central Iberian Zone, Zamora, Spain). *Am. Mineral.* **90**,1887-1899.

RODA-ROBLES, E., GALLISKI, M., NIZAMOFF, J., SIMMONS, W., KELLER, P., FALSTER, A. & HATERT, F. (2011): Cation partitioning between minerals of the triphylite ± graftonite ± sarcopside association in granitic pegmatites. *Asociación Geológica Argentina, Serie D, Publicación especial* **14**, 161-164.

RODA-ROBLES, E., GALLISKI, M., ROQUET, M.B., HATERT, F. & DE PARSEVAL, P. (2009): Phosphate mineral associations in the Cema pegmatite (San Luis Province, Argentina): paragenesis, chemistry and significance in the pegmatite evolution. *Estudos Geológicos* **19**(2), 300-304.

RODA-ROBLES, E., VIEIRA, R., PESQUERA, A. & LIMA, A. (2010): Chemical variations and significance of phosphates from the Fregeneda–Almendra pegmatite field, Central Iberian Zone (Spain and Portugal). *Mineral. Petrol.* **100**, 23-34.

ROQUET, M.B. (2010): *Mineralogía, geoquímica, tipología y relación con los granitoides de las pegmatitas del grupo Villa Praga-Las Lagunas, distrito Conlara, Sierra de San Luis.* Ph.D. thesis, Universidad Nacional de Córdoba, Córdoba, Argentina.

RUTHERFORD, M.J., HESS, P.C. & DANIEL, G.H. (1974): Experimental liquid line of descent and liquid immiscibility for basalt 70017. *Proc. 5th Lunar Sci. Conf.* **l**, 569-583.

SHIGLEY, J.E. & BROWN, G.E., JR. (1986): Lithiophilite formation in granitic pegmatites: a reconnaissance experimental study of phosphate crystallization from hydrous aluminosilicate melts. *Am. Mineral.* **71**, 356-366.

SIMS, J.P., SKIRROW, R.G., STUART-SMITH, P.G. & LYONS, P. (1997): Informe geológico y metalogenético de las Sierras de San Luis y Comechingones (provincias de San Luis y Córdoba), 1:250.000. Anales XXVIII. *Instituto de Geología y Recursos Minerales, SEGEMAR*, Buenos Aires, Argentina.

SMEDS, S. A., UHER, P., ČERNÝ, P., WISE, M.A., GUSTAFSSON, L. & PENNER. P. (1998): Graftonite–beusite in Sweden: primary phases, products of exsolution, and distribution in zoned populations of granitic pegmatites. *Can. Mineral.* **36**, 377-394.

THOMAS, R. & WEBSTER, J.D. (2000): Strong tin enrichment in a pegmatite-forming melt. *Mineral. Deposita* **35**, 570-582.

TIEN, T.Y. & HUMMEL, F.A. (1962): The system SiO_2–P_2O_5. *Am. Ceram. Soc., J.* **45**, 422-424.

VEKSLER, I. V., THOMAS, R. & WIRTH, R. (2003): Crystallization of $AlPO_4$–SiO_2 solid solutions from granitic melt and implications for P-rich melt inclusions in pegmatite quartz. *Am. Mineral.* **88**, 1724-1730.

VIGNOLA, P., DIELLA, V., OPPIZZI, P., TIEPOLO, M. & WEISS, S. (2008): Phosphate assemblages from the Brissago granitic pegmatite, western Southern Alps, Switzerland. *Can. Mineral.* **46**, 635-650.

VISSER, W. & KOSTER VAN GROOS, A.F. (1979): Effects of P_2O_5 and TiO_2 on liquid–liquid equilibria in the system K_2O–FeO–Al_2O_3–SiO_2. *Am. J. Sci.* **279**, 970-988.

WOLF, M.B. & LONDON, D. (1994): Apatite dissolution into peraluminous haplogranitic melts: an experimental study on solubilities and mechanisms. *Geochim. Cosmochim. Acta* **58**, 4127-4145.

WOLF, M.B. & LONDON, D. (1997): Boron in granitic magmas: stability of tourmaline in equilibrium with biotite and cordierite. *Contrib. Mineral. Petrol.* **130**, 12-30.

WYLLIE, P.J. & TUTTLE, O.F. (1964): Experimental studies of silicate systems containing two volatile components. II. The effects of SO_3, P_2O_5, HCl, and Li_2O, in addition to H_2O, on the melting temperatures of albite and granite. *Am. J. Sci.* **262**, 930-939.